THE JOURNAL OF BIOLOGICAL CHEMISTRY VOL. 280, NO. 47, pp. 39208–39219, November 25, 2005

C-terminal Tail Residue Arg^{1400} Enables NADPH to Regulate Electron Transfer in Neuronal Nitric-oxide Synthase*

Received for publication, July 18, 2005, and in revised form, August 29, 2005 Published, JBC Papers in Press, September 8, 2005, DOI 10.1074/jbc.M507775200

Mauro Tiso[‡§¶], David W. Konas[‡§], Koustubh Panda[‡§], Elsa D. Garcin[‖], Manisha Sharma[‡§], Elizabeth D. Getzoff[‖], and Dennis J. Stuehr[‡§1]

From the Departments of [‡]Immunology and [§]Pathobiology, Lerner Research Institute, Cleveland Clinic Foundation, Cleveland, Ohio 44195, the [¶]Department of Chemistry, Cleveland State University, Cleveland, Ohio 44115, and the [‖]Department of Molecular Biology and the Skaggs Institute for Chemical Biology, The Scripps Research Institute, La Jolla, California 92037

The neuronal nitric-oxide synthase (nNOS) flavoprotein domain (nNOSr) contains regulatory elements that repress its electron flux in the absence of bound calmodulin (CaM). The repression also requires bound NADP(H), but the mechanism is unclear. The crystal structure of a CaM-free nNOSr revealed an ionic interaction between Arg^{1400} in the C-terminal tail regulatory element and the 2′-phosphate group of bound NADP(H). We tested the role of this interaction by substituting Ser and Glu for Arg^{1400} in nNOSr and in the full-length nNOS enzyme. The CaM-free nNOSr mutants had cytochrome *c* reductase activities that were less repressed than in wild-type, and this effect could be mimicked in wild-type by using NADH instead of NADPH. The nNOSr mutants also had faster flavin reduction rates, greater apparent K_m for NADPH, and greater rates of flavin auto-oxidation. Single-turnover cytochrome *c* reduction data linked these properties to an inability of NADP(H) to cause shielding of the FMN module in the CaM-free nNOSr mutants. The full-length nNOS mutants had no NO synthesis in the CaM-free state and had lower steady-state NO synthesis activities in the CaM-bound state compared with wild-type. However, the mutants had faster rates of ferric heme reduction and ferrous heme-NO complex formation. Slowing down heme reduction in R1400E nNOS with CaM analogues brought its NO synthesis activity back up to normal level. Our studies indicate that the Arg^{1400}-2′-phosphate interaction is a means by which bound NADP(H) represses electron transfer into and out of CaM-free nNOSr. This interaction enables the C-terminal tail to regulate a conformational equilibrium of the FMN module that controls its electron transfer reactions in both the CaM-free and CaM-bound forms of nNOS.

Nitric oxide (NO)[2] has diverse biological functions and is generated in mammals by the NO synthase (NOS) enzymes (EC 1.14.13.39) (1, 2). Three NOS isozymes (inducible NOS or iNOS, neuronal NOS or nNOS, and endothelial NOS or eNOS) have evolved to function in health and disease (3–7). All are homodimeric enzymes that catalyze an NADPH- and O_2-dependent oxidation of L-arginine (Arg) to L-citrulline and NO (8, 9). Each NOS is composed of an N-terminal oxygenase domain that contains binding sites for iron protoporphyrin IX (heme), 6*R*-tetrahydrobiopterin, and Arg, and a C-terminal flavoprotein domain (NOSr) that contains binding sites for FAD, FMN, and NADPH (10, 11). The oxygenase and NOSr domains are connected by a calmodulin (CaM)-binding polypeptide (12, 13). CaM plays a critical role in activating NO synthesis, because its Ca^{2+}-dependent binding triggers electron transfer from the FMN hydroquinone to the ferric heme (14–18). This enables the heme to bind O_2 and initiate its reductive activation as required for NO synthesis (19, 20).

NOSr contains separate ferredoxin-$NADP^+$-reductase (FNR) and FMN modules (21, 22) and in this way is similar to a number of NADPH-utilizing dual flavin oxidoreductases (23–27). In NOSr, a hydride transfer occurs from NADPH to FAD within the FNR module, followed by electron transfer from the FAD hydroquinone to FMN (17, 28, 29). The reduced FMN module (containing FMN hydroquinone) is then thought to swing away from the FNR module to transfer electrons to the NOS ferric heme or to exogenous acceptors like cytochrome *c* (Fig. 1*A*) (30, 31). According to this model, the steady-state activity of nNOSr is determined in part by a conformational equilibrium that determines the probability and extent to which the FMN module interacts with its electron donor (FNR) and the electron acceptor (NOS heme or cytochrome *c*). Recent reports suggest that NADP(H) binding shifts the set point for the conformational equilibrium to favor an "FMN shielded" form of nNOSr that has repressed cytochrome *c* reductase activity (32–34). CaM shifts the conformational equilibrium in the opposite direction to favor a deshielded FMN module that is associated with increased cytochrome *c* reductase activity. Notably, a single point mutation within nNOSr reverses the effect of NADP(H) binding such that it then mimics CaM in influencing the conformational equilibrium of nNOSr and its catalysis (34). These results imply a finely tuned regulation of FMN module reactivity in nNOSr.

Studies with NOS chimeras established that the identity of NOSr determines the ferric heme reduction rate in a given NOS (35–37). At least three unique regulatory elements are present in NOSr. They are an autoinhibitory helix, represented by a 42- to 45-amino acid insert in the FMN module of eNOS and nNOS (38, 39), a CD2A loop, which is a short amino acid insertion in the connecting domain of constitutive NOS (40), and a C-terminal tail, correspondent to a 33-amino acid extension in nNOS and extensions of similar length at the C termini of eNOS and iNOS (41, 42). Deletion studies indicated that the regulatory elements help to repress electron flux into and out of NOSr in the CaM-free state and may help to relieve the repression upon CaM binding (41–46). Although these studies established a basic framework for regulation in nNOSr, they could not discern the physical basis for the effects nor address their potential relationships.

A recent crystal structure of an intact, CaM-free nNOSr (Protein Data Bank Code 1TLL) has revealed how certain regulatory elements

* This work was supported by National Institutes of Health Grants GM51491 (to D. J. S.) and R01HL5883 (to E. D. Getzoff) and by American Heart Association fellowship 0415154B (to M. T.). The costs of publication of this article were defrayed in part by the payment of page charges. This article must therefore be hereby marked "*advertisement*" in accordance with 18 U.S.C. Section 1734 solely to indicate this fact.

[1] To whom correspondence should be addressed: Dept. of Immunology, NB-30, The Cleveland Clinic Foundation, 9500 Euclid Ave., Cleveland, OH 44195. Tel.: 216-445-6950; Fax: 216-444-9329; E-mail: stuehrd@ccf.org.

[2] The abbreviations used are: NO, nitric oxide; nNOS, neuronal nitric-oxide synthase; nNOSr, flavoprotein domain of neuronal nitric-oxide synthase; CaM, calmodulin; P_i, phosphate; EPPS, 4-(2-hydroxyethyl)-1-piperazinepropanesulfonic acid; SCaM, soybean calmodulin; TnC, cardiac troponin C; FNR, ferredoxin-$NADP^+$-reductase.

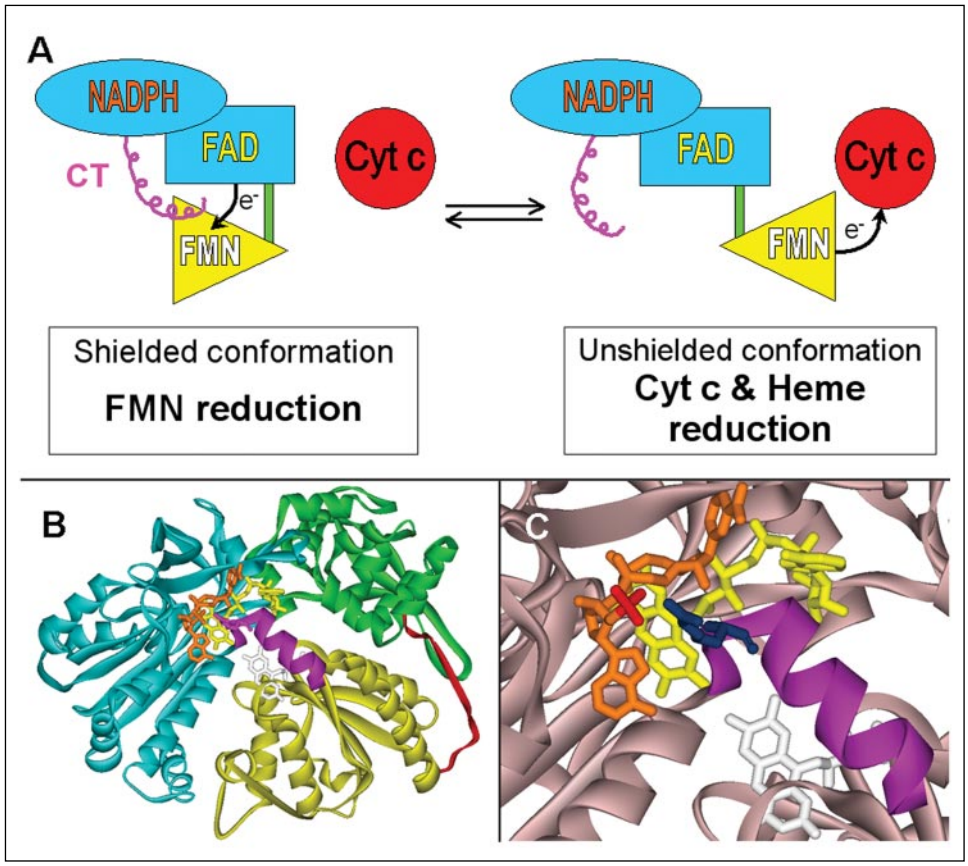

FIGURE 1. **Conformational equilibrium of the nNOSr FMN module and basis for its regulation by Arg[1400] and bound NADPH.** *A*, the *diagram* illustrates a conformational equilibrium that may control the electron transfer reactions of the FMN module (*yellow*). The module is expected to swing back and forth to contact the FNR module (*blue*) and an electron acceptor like cytochrome *c* or NOS heme (*red*). The C-terminal tail (pink) is thought to affect the equilibrium by physically stabilizing the FMN-shielded conformation. *B*, *ribbon diagram* of the nNOSr structure that highlights the position of the C-terminal tail helix (*pink*), FMN module (*yellow*), hinge (*red*), connecting domain (*green*), FNR domain (*teal*), bound cofactors NADP(H) (*orange*), FAD (*yellow*), and FMN (*white*), the Arg^{1400} residue (*purple*), and the 2′-P_i of NADP(H) (*red*). *C*, close-up view to emphasize the Arg^{1400}-2′-P_i interaction.

may repress electron transfer (30). Specifically, the position of the C-terminal tail helix suggests that it physically restrains the FMN module from moving away from the FNR module as required for its electron transfer functions (Fig. 1*B*). A closer view reveals that the C-terminal tail residue Arg^{1400} makes an ionic interaction with the negatively charged 2′-phosphate group of bound NADP(H) (Fig. 1*C*). We therefore hypothesized that Arg^{1400} enables an interaction between bound NADP(H), the C-terminal tail, and the FMN module that could conceivably link NADP(H) binding to repression of FMN electron transfer in CaM-free nNOS. In the current report, we explore this hypothesis by characterizing mutants of nNOSr and full-length nNOS enzymes that contain amino acid substitutions designed to either eliminate the charge interaction between Arg^{1400} and the 2′-P_i of NADPH, or switch it to a charge-repelling interaction.

EXPERIMENTAL PROCEDURES

Materials and General Methods—All reagents and materials were obtained from Sigma or sources previously reported (47, 48). Human CaM point mutant M144V, soybean CaM isoform proteins SCaM-1, SCaM-4, and SCaM-5, and the CaM-cardiac troponin C chimeras CaM1TnC (number refers to the CaM domain that is replaced by an analogous TnC domain in the chimera) were expressed in *Escherichia coli* and purified to homogeneity by Ca^{2+}-dependent phenyl-Sepharose (Amersham Biosciences) column chromatography as previously described (49–52). SCaM-1 point mutant V144M was a gift from Dr. J. David Johnson, Biochemistry Dept., Ohio State University.

UV-visible spectra and steady-state kinetic data were recorded on a Hitachi U2000 spectrophotometer or Varian Cary 100 Bio spectrophotometer using a quartz cuvette with a 1-cm path length. Single wavelength stopped-flow kinetic experiments were performed using a Hi-Tech (Salisbury, U.K.) SF-51MX instrument equipped for anaerobic work and photomultiplier detection. Full-spectra stopped-flow experiments were performed using a Hi-Tech SF-61 instrument equipped for anaerobic work and rapid-scanning diode array detection. The buffer used for all experiments and protein purifications (Buffer A) unless noted otherwise contained 40 mM EPPS (pH 7.6), 10% glycerol, and 150 mM NaCl. When necessary, samples were made anaerobic in an air-tight cuvette by repeated cycling of vacuum followed by a positive pressure of catalyst-deoxygenated nitrogen. The nNOS reductases were prepared for use by oxidizing the purified air-stable semiquinone form with potassium ferricyanide followed by passing the mixture through a PD-10 desalting column.

Molecular Biology—Restriction digestions, cloning, bacterial growth, transformation, and isolation of DNA fragments were performed using standard techniques. Originally rat nNOS DNA was inserted into the pCWori vector at 5′-NdeI and 3′-XbaI restriction sites. The R1400S and R1400E mutation sites in the nNOS cDNA were constructed by subcloning a PCR-generated fragment from the pCWori/nNOS using a 5′-oligonucleotide constructed as previously reported (34, 53). The nNOS cDNA fragment coding from the KpnI unique restriction site at position 4170 to the XbaI restriction site at position 4441 was amplified using primers as follows: R1400S forward primer, AAC CGG TAC CAC GAG GAC ATC TTT GGA GTC ACC CTC **AGC** ACG; R1400E forward primer, AAC CGG TAC CAC GAG GAC ATC TTT GGA GTC ACC CTC **GAA** ACG. The reverse primer in both cases was AAA TCT AGA AGG ACC AGG ACA CAG CAA CAG GAC AAG. Mutations are denoted in bold; silent restriction sites are underlined. The sequences of mutations were confirmed at the Cleveland Clinic DNA sequencing facility, and DNA containing the desired mutation was transformed into *E. coli* BL21(DE3) cells for protein expression. These

cells were also transformed with a pACYC plasmid containing human CaM and selected with chloramphenicol to co-express CaM with the nNOS protein.

Expression and Purification—The nNOSr domain (construct 695–1429) has been purified by sequential chromatography on a 2′,5′-ADP-Sepharose affinity column and CaM-Sepharose resin following a procedure recently published (34). The protein was dialyzed against buffer A (see "Experimental Procedures") and stored in aliquots at −80 °C. Purity of the protein was assessed by SDS-PAGE and spectral analysis. The flavin content of the nNOSr proteins was obtained by boiling a known amount of nNOSr protein for 3 min followed by short centrifugation and determination of the flavin concentration in the supernatant using an extinction coefficient of 12.2 mM^{-1} cm^{-1} at 447 nm. The full-length wild-type and mutant nNOS proteins were overexpressed in *E. coli* strain BL21(DE3) containing a His_6 tag in the N termini to aid purification in a Ni-resin affinity column (54). The protein concentration was estimated by quantification of heme protein content as evidenced through the formation of the ferrous-CO adduct with an absorption maxima at 444 nm (55).

NO Synthesis, NADPH Oxidation, and Cytochrome c Reduction—Steady-state activities were determined separately at room temperature as previously described (15, 55). In the case of NO synthesis and NADPH oxidation the oxyhemoglobin assay buffer solution contains also 150 mM NaCl.

Measurement of Apparent K_m and K_{cat} for NADPH and NADH—Apparent K_m and k_{cat} values of wild-type and mutants nNOS enzymes were determined in the presence or absence of bound Ca^{2+}/CaM by analysis of cytochrome *c* reduction measured at 550 nm using quartz cuvettes or a 96-microwell Molecular Dynamics kinetic plate reader. Assays were run at 25 °C in 40 mM EPPS, pH 7.6, containing 4 μM FAD, 4 μM FMN, 0.1 mg/ml bovine serum albumin, 70 μM cytochrome *c*, 0.6 mM EDTA, or 0.8 mM Ca^{2+}, and 0.1 μM CaM and variable concentrations of NADPH (0.5–15 μM) or NADH (0.33–10 mM). Assay volumes were 0.66 ml for cuvettes and 0.2 ml for microwell plates. Reactions were started by adding 1.5 nM enzyme. Data were fitted to the classic Michaelis-Menten equation for analyzing the enzyme kinetics using the software Origin® version 6.1.

Auto-oxidation of Reduced nNOSr—A solution of nNOSr protein (8–10 μM) containing EDTA (0.5 mM) in air-saturated buffer was reduced by adding excess NADPH (200 μM) and then allowed to auto-oxidize at room temperature in an open cuvette. The process was monitored at 457 nm, and visible spectra at indicated time points (see "Results") were recorded in similar experiments.

Anaerobic Stopped-flow Flavin Reduction Kinetics—The absorbance changes associated with nNOSr flavin reduction by NADPH were recorded at 10 °C in the single-wavelength stopped-flow instrument by rapidly mixing a solution of oxidized nNOSr (6–8 μM) containing either EDTA (1 mM) or $CaCl_2$ (2 mM) plus CaM (18–24 μM) with a solution of 60–100 μM NADPH (excess NADPH). For each protein sample used the maximum absorbance value at 457 nm was obtained by replacing the NADPH solution in one of the stopped-flow syringes with buffer only and recording two to three additional mixing events. The individual rate constants were first estimated by analyzing experiments of different time duration. The final reported values were obtained by fitting to a quadruple exponential function experiments at a 2-s time scale, which captures all four rate constants. The residuals were minimized, and the signal-to-noise ratio was improved by averaging four to five individual mixing experiments. Percent absorbance changes were calculated for the absorbance change occurring in the instrument dead time (1.5 ms), and each kinetic phase was calculated as the ratio between the total absorbance change and the relative ΔAbs (absorbance change) value of each kinetics phase as obtained from the fitting program.

Anaerobic Pre-steady-state Cytochrome c Reduction—A solution of nNOSr (16 μM), glycine (3 mM), 5-deazariboflavin (catalytic), and either EDTA (1 mM) or $CaCl_2$ (2 mM) plus CaM (30 μM) was completely photoreduced in an anaerobic cuvette using a commercial slide projector bulb until no changes in the UV-visible spectrum of the sample were observed upon further irradiation of the sample. The pre-reduced protein sample was rapidly mixed in the stopped-flow spectrophotometer with a solution of cytochrome *c* (4 μM) at 10 °C, and the absorbance changes at 550 nm were recorded. In some cases 1 mM NADPH was added to the pre-reduced protein sample, and the mixture was incubated at 10 °C for at least 15 min prior to mixing. Absorbance data were then fit to a single exponential function.

Heme Reduction of Full-length Proteins—Kinetics of heme reduction was analyzed at 10 °C as described previously (56). Reactions were initiated by mixing an anaerobic, buffered, CO-saturated solution containing 100 μM NADPH with 4 μM nNOS (wild-type or mutant) prepared under anaerobic conditions in 100 mM EPPS, pH 7.6, containing 150 mM NaCl, 10 μM 6*R*-tetrahydrobiopterin, 0.4 mM dithiothreitol, 1 mM Arg, and 10 μM CaM, or 20 μM soybean or chimeras CaM isoforms. Heme reduction was followed by formation of the ferrous-CO complex at 444 nm. The time course of absorbance changes was fit to a single exponential equation using a nonlinear least square method provided by the instrument manufacturer. The initial spectrum recorded without NADPH was used as a baseline. Signal-to-noise ratio was improved by averaging data from multiple individual mixing experiments.

Kinetics of Heme-NO Complex Formation—Experiments were done at 10 °C in a SF-61 Hi-Tech stopped-flow apparatus. To initiate NO synthesis an air-saturated solution that contained 100 mM EPPS, pH 7.6, 5 μM nNOS or mutant, 150 mM NaCl, 10 μM 6*R*-tetrahydrobiopterin, 0.4 mM dithiothreitol, 1 mM Arg, 0.5 mM EDTA, 1.2 mM Ca^{2+}, and 10 μM CaM was rapidly mixed with a buffered solution containing 50 μM NADPH. Absorbance at 436 nm was monitored to follow ferrous heme-NO formation, and absorbance at 340 nm was monitored to follow NADPH oxidation (56, 57). Signal-to-noise ratios were improved by averaging four to six consecutive scans. Each experiment was performed three separate times.

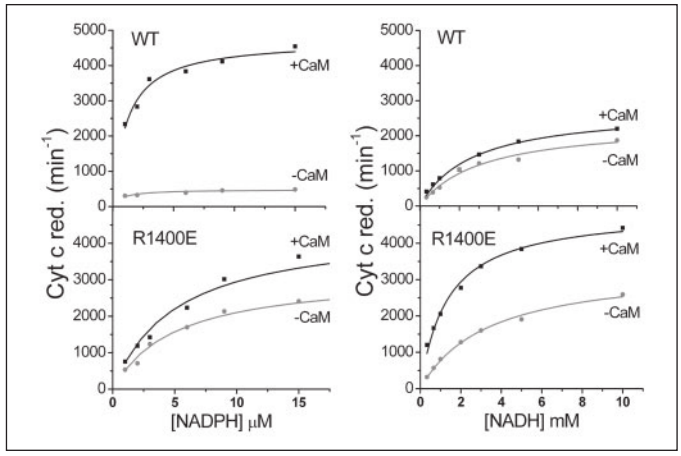

FIGURE 2. **Cytochrome *c* reductase activity of wild-type nNOSr and the R1400E mutant *versus* NADPH or NADH concentration.** The *points* are the mean initial velocity obtained at each dinucleotide concentration indicated, and the *lines* are a fit of the data to the Michaelis-Menten equation. The reactions contained 1.5 nM enzyme and were run at room temperature in the absence or presence of CaM as described under "Experimental Procedures." Each experiment was performed in triplicate, and values are representative of two or more independent determinations.

TABLE ONE

Apparent k_{cat} values for cytochrome c reductase activities supported by NADPH or NADH in wild-type nNOSr and the Arg^{1400} mutants

The apparent k_{cat} values were calculated from cytochrome *c* reductase activities determined at 25 °C as described under "Experimental Procedures." Mean data from triplicate experiments were fit to the Michaelis-Menten equation. Values ± S.D. are representative of two or more independent enzyme preparations and are expressed as moles of product formed per mole of heme per min.

nNOSr enzyme	NADPH		NADH	
	−CaM	+CaM	−CaM	+CaM
	min^{-1}			
Wild-type	499 ± 22	4993 ± 178	2379 ± 198	2780 ± 174
R1400S	1100 ± 88	4380 ± 189	4200 ± 224	5034 ± 213
R1400E	3114 ± 200	4413 ± 200	3377 ± 245	4900 ± 170

TABLE TWO

Apparent K_m values for NADPH and NADH for the nNOSr enzymes

Apparent K_m values were calculated from cytochrome *c* reductase activities determined at 25 °C in assays run in the presence or absence of CaM and containing different concentrations of NADPH or NADH. Data from triplicate experiments were fit to the Michaelis-Menten equation as described under "Experimental Procedures." Values are the mean ± S.D. and are representative of three independent measurements each.

nNOSr enzyme	K_m of NADPH		K_m of NADH	
	−CaM	+CaM	−CaM	+CaM
	μM			
Wild-type	1.0 ± 0.2	1.5 ± 0.3	3110 ± 600	2670 ± 410
R1400S	2.7 ± 0.5	4.9 ± 1.1	5520 ± 570	2310 ± 340
R1400R	5.0 ± 0.9	5.1 ± 0.7	3360 ± 320	1340 ± 170

Analysis of Stopped-flow Data—In most cases, the spectral traces were fit according to single or multiple exponential equations, with the residuals for each fit determined by the software. The best fit was designated when adding further exponentials did not improve the fit as judged by the residuals. In the case of flavin reduction by excess NADPH, we used a four exponential equation to fit the absorbance change at 457 nm, as done in previous reports (34, 58).

RESULTS

Mutant Protein Expression and Characterization—R1400E and R1400S mutants were expressed both as nNOSr and full-length nNOS enzymes. The nNOSr enzymes were obtained in about 3-fold greater yield than the full-length proteins. All enzymes were found to have 2 mol of flavin incorporated (FAD plus FMN) per mole of protein (data not shown). Spectrophotometric analysis of the full-length proteins showed that 6*R*-tetrahydrobiopterin and Arg binding caused their heme Soret bands to shift to a high spin state, and reduction of the enzymes in the presence of CO produced the expected 444 nm Soret absorbance peak for the ferrous heme-thiolate CO complex (data not shown). These findings indicate that the mutations at Arg^{1400} do not grossly perturb enzyme structure, prosthetic group and substrate binding, or heme electronic environment.

Interactions of nNOSr Enzymes with NADPH and NADH Cofactors—We investigated the importance of Arg^{1400} interaction with the 2′-P_i group of NADPH by measuring cytochrome *c* reductase activities in reactions that were supported either by NADPH or NADH. Fig. 2 shows representative plots of initial velocity *versus* dinucleotide substrate concentrations for the wild-type and R1400E nNOSr enzymes (data for R1400S nNOSr is not shown). TABLE ONE contains the apparent k_{cat} values obtained for these experiments. In the NADPH-supported reactions the wild-type and Arg^{1400} mutant enzymes had similar apparent k_{cat} values in the CaM-bound state. However, the apparent k_{cat} of the CaM-free wild-type was suppressed 10-fold relative to its CaM-bound value, consistent with previous reports (39, 55). This difference decreased to a 4-fold suppression in CaM-free R1400S nNOSr, and to less than a 2-fold suppression in CaM-free R1400E nNOSr. In the NADH-driven reactions, the apparent k_{cat} values for CaM-free enzymes ranged from 69 to 83% that of the values obtained in the CaM-bound state. This indicates there was less suppression when the reactions were supported by NADH. Thus, both Arg^{1400} and the 2′-P_i group of NADPH are important for repressing the cytochrome *c* reductase activity of CaM-free nNOSr.

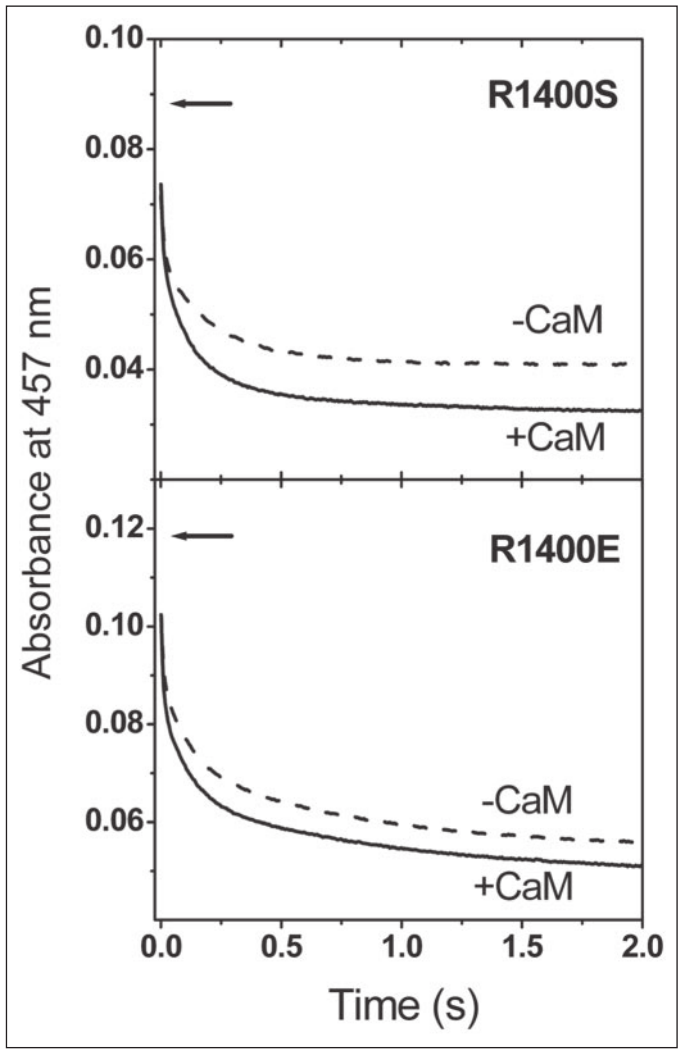

FIGURE 3. **Absorbance traces describing the kinetics of NADPH-dependent flavin reduction in the R1400E and R1400S nNOSr mutants in the absence and presence of CaM.** Stopped-flow traces were collected at 457 nm by rapidly mixing a solution of oxidized R1400S (*top*) or R1400E (*bottom*) nNOSr with an excess of NADPH at 10 °C as described under "Experimental Procedures." The initial absorbance value is indicated in *each panel* by the *arrow*. The *traces* shown are an average of five individual scans and are representative of two independent experiments. The calculated best-fit lines were indistinguishable from the experimental traces.

TABLE TWO contains apparent K_m values for NADPH and NADH as determined from the cytochrome *c* reductase assays. The R1400S and R1400E mutants had apparent K_m values for NADPH that were two- to five-times greater than the value for wild-type nNOSr in the presence or absence of CaM. The apparent K_m values for NADH ranged from 1 to 5 mM for the three enzymes. These results confirm that the 2′-P_i group is important for discriminating between NADPH and NADH binding in nNOSr but suggest that the Arg^{1400}-2′-P_i interaction is a minor contributor to this process.

TABLE THREE

Kinetic analysis of NADPH-dependent flavin reduction in the nNOSr enzymes

Reactions were run under anaerobic conditions in a stopped-flow instrument at 10 °C. Reactions were initiated by mixing oxidized enzyme with a 10-fold excess of NADPH. The absorbance change at 457 nm was fit to a quadruple exponential function as described under "Experimental Procedures."

Protein	Conditions	Absorbance change[a]	k_1[b]	k_2[b]	k_3[b]	k_4[b]
Wild-type[c]	−CaM	27	40 ± 5.3 (12)	3.0 ± 0.16 (29)	0.71 ± 0.04 (21)	0.026 ± 0.006 (11)
Wild-type[c]	+CaM	25	151 ± 9.4 (13)	13.0 ± 0.60 (26)	4.4 ± 0.41 (20)	0.090 ± 0.017 (16)
R1400S	−CaM	30	78 ± 2.6 (25)	12.3 ± 1.9 (4)	4.2 ± 0.08 (33)	0.109 ± 0.011 (8)
R1400S	+CaM	20	126 ± 7.2 (25)	19.8 ± 2.8 (10)	5.8 ± 0.08 (33)	0.211 ± 0.007 (12)
R1400E	−CaM	20	134 ± 5.2 (18)	9.4 ± 0.3 (21)	1.2 ± 0.13 (21)	0.05 ± 0.02 (20)
R1400E	+CaM	35	130 ± 4.6 (20)	16.4 ± 0.4 (19)	1.7 ± 0.09 (12)	0.10 ± 0.01 (14)

[a] Percentage of the total absorbance change occurring in the instrument dead time.
[b] Rate constants are reported as the calculated rate (s^{-1}) along with the percentage (in parenthesis) of the total absorbance change for this process.
[c] Data from Ref. 34.

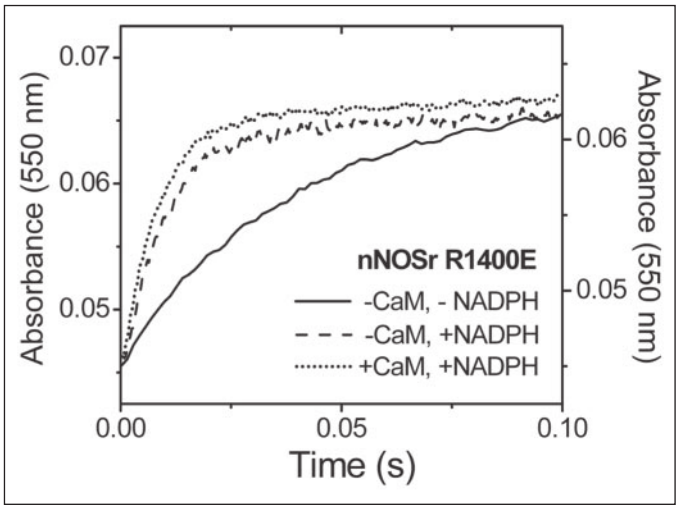

FIGURE 4. **Absorbance traces illustrating the effect of NADPH and CaM on the kinetics of electron transfer to cytochrome *c* by photoreduced R1400E nNOSr.** Anaerobic, photoreduced enzyme was prepared under the indicated conditions and then rapid-mixed with a sub-stoichiometric amount of cytochrome *c* in the stopped-flow instrument at 10 °C as described under "Experimental Procedures." Absorbance changes were recorded at 550 nm. *Traces* shown are an average of four or five individual scans and are representative of two independent experiments. Rate constants obtained in this manner were used in the preparation of Fig. 5.

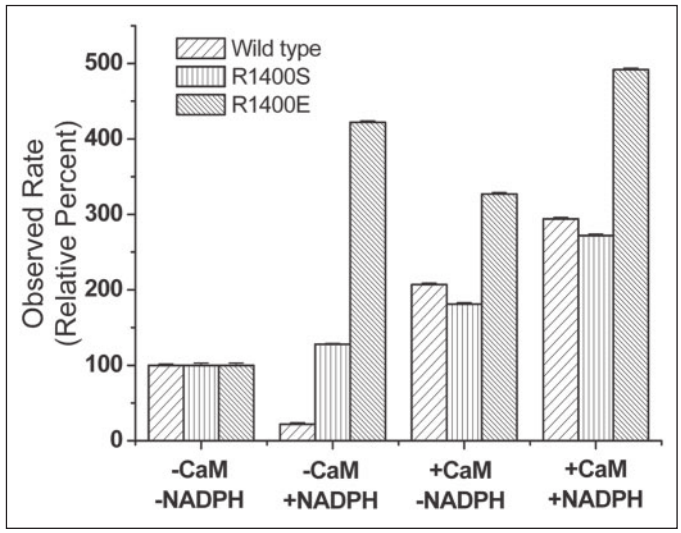

FIGURE 5. **Comparative electron transfer rates to cytochrome *c* as catalyzed by the pre-reduced wild-type and mutant nNOSr under various conditions.** The rate constants we obtained in pre-steady-state cytochrome *c* reduction experiments (as described in Fig. 4) for each CaM- and NADPH-free enzyme were set to equal 100%, and the rates obtained under all other indicated reaction conditions were expressed as relative percentages of the basal value for each enzyme. The *bars* are the mean ± S.D. and indicate the effects of CaM and NADPH binding on the electron transfer to cytochrome *c* by each enzyme.

TABLE FOUR

Effect of CaM and NADPH on the rate of electron transfer to cytochrome c by pre-reduced nNOSr and the Arg[1400] mutant enzymes

Anaerobic enzymes were photo-reduced under the indicated conditions of CaM and NADPH binding and were rapidly mixed at 10 °C in a stopped-flow spectrophotometer with a substoichiometric amount of cytochrome *c*, as detailed under "Experimental Procedures." The absorbance gain at 550 nm was used to calculate the observed rate of electron transfer to cytochrome *c* under each condition. The rates (s^{-1}) are the mean ± S.D. of five to six mixing experiments done with two independent preparations.

nNOSr enzyme	−CaM −NADPH	−CaM +NADPH	+CaM −NADPH	+CaM +NADPH
Wild-type	13.3 ± 0.2	2.9 ± 0.06	27.3 ± 0.2	38.8 ± 0.4
R1400S	28.4 ± 0.8	36.5 ± 0.6	51.6 ± 1.0	77.5 ± 1.3
R1400E	22.8 ± 0.3	96.3 ± 0.9	74.6 ± 1.0	112.2 ± 1.0

Kinetics of Flavin Reduction by NADPH—We investigated the kinetics of NADPH-dependent flavin reduction in the Arg[1400] mutants in the presence or absence of CaM. Representative single wavelength stopped-flow traces obtained at 457 nm during reduction of R1400S or R1400E nNOSr with excess NADPH are shown in Fig. 3 (corresponding results for the wild-type nNOSr were recently reported) (34). All stopped-flow traces fit well to a quadruple exponential function, and thus four rate constants were obtained using the process described under "Experimental Procedures." For each experiment an initial absorbance value representing no flavin reduction was also obtained (Fig. 3). Data are summarized in TABLE THREE. A significant amount of the total absorbance change took place in the dead time of the instrument in all reactions, consistent with previous reports (32, 34, 53). Under CaM-free conditions, the kinetics of flavin reduction in R1400S nNOSr was faster than in wild-type nNOS. This was evidenced by the mutant k_1, k_2, k_3, and k_4 transitions having 2- to 6-times higher values. CaM binding to R1400S nNOSr further increased the rates of all four transitions such that they became similar (although higher) to those of the CaM-bound, wild-type nNOSr. The kinetics of flavin reduction in the CaM-free R1400E mutant was also faster than in CaM-free wild-type nNOSr. In fact, there was very little difference in the rates obtained for the CaM-bound and CaM-free R1400E mutant, and these rates were in turn very similar to those of the CaM-bound wild-type nNOSr. Thus, in the CaM-free state, flavin reduction kinetics are less repressed in the R1400S mutant, and not repressed in the R1400E mutant, relative to wild-type nNOSr.

Pre-steady-state Cytochrome c Reduction—NADPH binding to CaM-free nNOSr causes a greater shielding of its FMN module, and this is

thought to explain the repressed catalysis of cytochrome *c* reduction that is a characteristic of the CaM-free state (17, 32, 34). To determine if the R1400 mutants lack this regulation, we measured rates of electron transfer between the photo-reduced nNOSr proteins and cytochrome *c* under pseudo-first order conditions (using excess nNOSr proteins) and compared how CaM and NADPH binding would affect the rates. Previous work in similar experimental systems had shown that NADPH binding to CaM-free nNOSr inhibited its rate of electron transfer to cytochrome *c*, whereas CaM binding increased the rate (32, 34). Fig. 4 contains some representative stopped-flow traces recorded at 550 nm in the R1400E nNOSr reactions, which indicate the rates of electron transfer to cytochrome *c* under the various conditions. Each trace fits well to a mono-exponential curve. Observed rates obtained for the three nNOSr enzymes are summarized in TABLE FOUR. To facilitate comparison (34), the rate we obtained for each CaM- and NADPH-free enzyme was set to 100%, and the rates obtained under all other reaction conditions were expressed as relative percentages of this basal value (Fig. 5). We observed a 5-fold rate decrease associated with NADPH binding to CaM-free wild-type nNOSr, consistent with previous reports (32, 34). Conversely, NADPH binding was associated with rate increases of 1.3- and 4.2-fold in the R1400S and R1400E mutants, respectively. CaM binding caused rate increases in all three enzymes, regardless of their NADPH binding. The data identify Arg^{1400} as an essential component in the mechanism by which bound NADPH represses electron transfer from the FMN module of nNOSr. When Arg^{1400} is switched to Ser or Glu, NADPH appears to stabilize a conformation of nNOSr that better facilitates electron transfer from its FMN module.

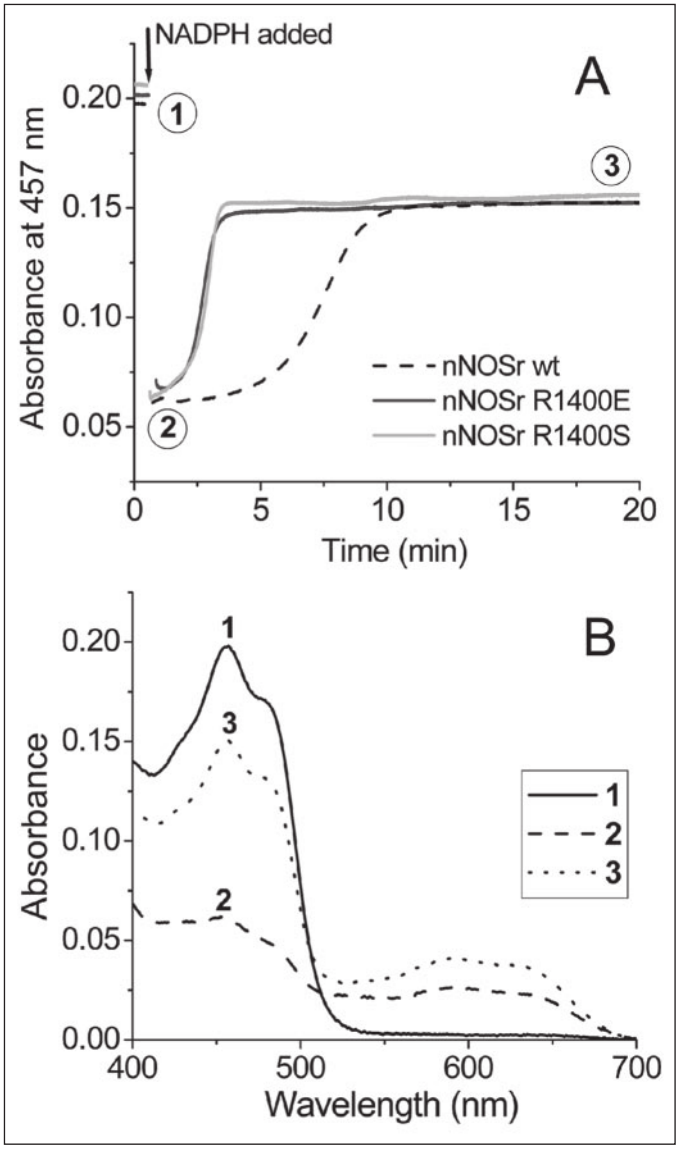

FIGURE 6. **Kinetics of flavin auto-oxidation in the NADPH-reduced wild-type and mutant nNOSr enzymes.** Wild-type and mutant nNOSr proteins were diluted to 9 μM in air-saturated buffer in a cuvette, given a 20-fold molar excess of NADPH, and then allowed to consume NADPH at room temperature as described under "Experimental Procedures." *A*, the redox status of enzyme flavins was monitored at 457 nm *versus* time. *B*, the visible spectra shown were recorded for the R1400E nNOSr prior to NADPH addition (*1*), during NADPH consumption (*2*), and after all the NADPH had been consumed and flavin reoxidation had occurred (*3*). Data are representative of two independent experiments.

Stability of Reduced Flavins—Mutations in the C-terminal tail of nNOSr have been shown to increase the reactivity of its reduced flavins with O_2 (34, 42, 56). To determine if the Arg^{1400} mutations altered the air stability of the reduced flavins, we treated the fully oxidized R1400E, R1400S, or wild-type nNOSr enzymes with a 20-fold excess of NADPH in air-saturated buffer and then monitored the time required for each enzyme to consume the NADPH and then reoxidize. Fig. 6 (*upper panel*) shows the time course of flavin reoxidation as monitored at 457 nm. The R1400E and R1400S mutants both consumed the NADPH about 5 times faster than did wild-type nNOSr. Once the NADPH was oxidized, the absorbance gains indicated that reduced flavins in the 1400E and R1400S mutants reoxidized at 3-fold faster rates compared with wild-type. However, after 20 min the final absorbance values at 457 nm were similar in all three enzymes, indicating that the final state of their flavins was the same. Fig. 6 (*lower panel*) contains visible spectra that were recorded at three points indicated during the course of the R1400E nNOSr reaction. The spectra are similar to those observed during the wild-type nNOSr reaction (59, 60) and indicate that the R1400E mutant reoxidized to a stable, one-electron reduced form that contains a flavin semiquinone radical. We conclude that the Arg^{1400} mutations increase the O_2 reactivity of reduced flavin species in nNOSr but do not alter the stability of its one-electron reduced form.

NO Synthesis and NADPH Oxidation—We utilized full-length nNOS enzymes to investigate how the Arg^{1400} mutations affect NO synthesis, NADPH oxidation, and related parameters. Their steady-state NO synthesis and associated NADPH consumption activities are listed in

TABLE FIVE

Steady-state NO synthesis activities and associated NADPH oxidation rate for wild-type nNOS and the Arg^{1400} mutants

Rates of NO synthesis and NADPH oxidation are expressed as moles of product per mole of heme per min and were derived from assays run at room temperature as described under "Experimental Procedures." The values are the mean ± S.D. of three separate measurements, two enzyme preparations each.

nNOSfl enzyme	NO synthesis from NOHA (+CaM)	NO synthesis from Arg		NADPH oxidation in the Arg reaction	
		+CaM	−CaM	+CaM	−CaM
Wild-type	91.2 ± 4.7	51.2 ± 3.1	Nil	107.0 ± 8.8	3.0 ± 1.1[a]
R1400S	61.6 ± 2.0	34.3 ± 2.8	Nil	109.1 ± 2.4	10.0 ± 2.5
R1400E	40.9 ± 1.1	29.4 ± 2.1	Nil	111.3 ± 5.5	13.8 ± 3.0

[a] Value is from Ref. 55.

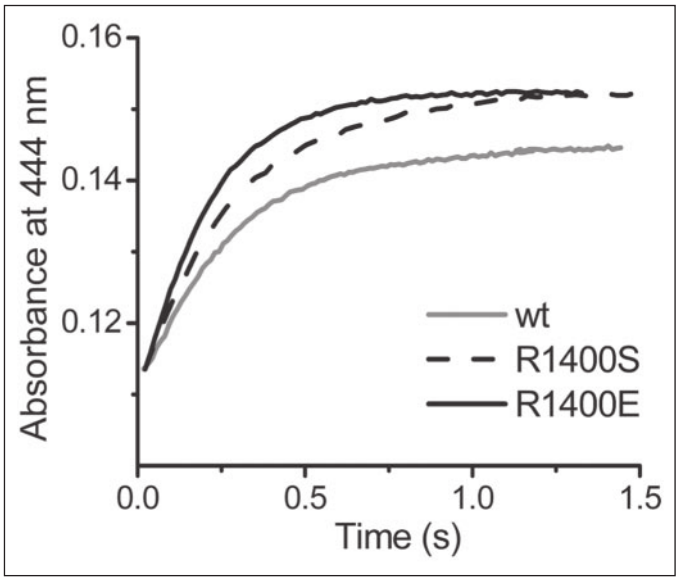

FIGURE 7. **Stopped-flow analysis of ferric heme reduction in CaM-bound wild-type and mutant nNOS enzymes.** Anaerobic, CaM-bound enzymes were rapidly mixed with excess NADPH to trigger flavin and heme reduction at 10 °C in anaerobic, CO-saturated buffer as described under "Experimental Procedures." Ferric heme reduction was determined from the rate of ferrous-CO complex formation at 444 nm. *Traces* best fit to a single exponential equation. The *traces* shown are the average of six individual scans and are representative of multiple independent experiments with three batches of enzyme.

TABLE FIVE. The CaM-free R1400S and R1400E mutants had no detectable NO synthesis activities, although their NADPH oxidase activities were three to four times faster than in wild-type nNOS. The NO synthesis activities of the CaM-bound mutants were lower than the wild-type value, with rank order wild-type > R1400S > R1400E. This relationship held whether Arg or NOHA served as substrate. The NADPH oxidation rates that were associated with NO synthesis from Arg were similar in all three enzymes, indicating that a greater portion of NADPH oxidation was uncoupled from NO release in the mutants. This suggested that the Arg[1400] mutations affect the electron transfer to the nNOS ferric heme.

Anaerobic Heme Reduction—We next compared rates of ferric heme reduction in the mutant and wild-type nNOS enzymes. Heme reduction was monitored by following the formation of the ferrous heme-CO complex at 444 nm (Fig. 7). Ferric heme reduction was monophasic in all three enzymes, and the rates of heme reduction were 5.1 ± 0.3 (n = 4) (ranged from 4.8 to 5.6) in R1400E nNOS, 4.7 ± 0.2 (n = 3) (ranged from 4.4 to 5.2) in R1400S nNOS, and 3.9 ± 0.1 (n = 4) (ranged from 3.8 to 4.2) in wild-type nNOS preparations. Thus, the mutant rates of ferric heme reduction were consistently faster than in wild-type nNOS, with rank order R1400E > R1400S > wild-type.

Ferrous Heme-NO Complex Formation and NADPH Consumption during NO Synthesis—If the Arg[1400] mutants have faster rates of ferric heme reduction, then they should have faster rates of ferrous heme-NO complex formation during the initial phase of their NO synthesis reactions (56). We therefore monitored heme-NO complex formation and NADPH consumption after initiating NO synthesis at 10 °C in the stopped-flow diode-array spectrophotometer. Fig. 8 contains data from reactions catalyzed by wild-type nNOS and each Arg[1400] mutant. The spectral traces in the main panels were recorded during steady-state NO synthesis (*solid line*) and after NO synthesis terminated due to NADPH depletion (ferric enzyme, *dashed line*). These indicate there was a buildup of a ferrous heme-NO complex absorbing at 436 nm in the three enzyme reactions. The *insets* show the absorbance changes at 436 and 340 nm during the first 5 s of reaction (pre-steady state catalysis)

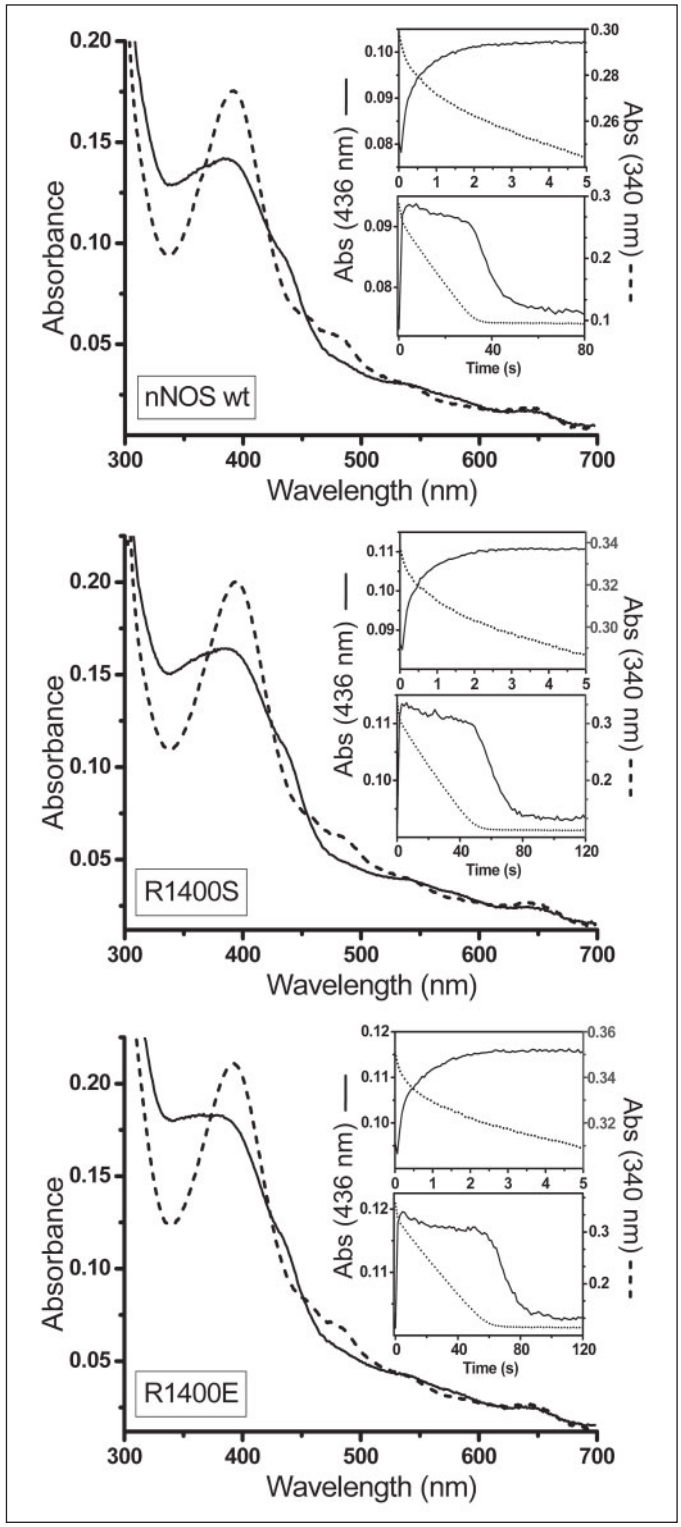

FIGURE 8. **Kinetics of ferrous-NO complex formation and NADPH oxidation during NO synthesis by wild-type and mutant nNOS enzymes.** An air-saturated solution containing ~5 μM CaM-bound enzyme, Arg, and cofactors was rapidly mixed at 10 °C with a solution of buffer containing 30 or 50 μM NADPH, and sequential spectra were recorded in the stopped-flow spectrophotometer. *Top*, nNOS wild type. *Middle*, R1400S mutant. *Bottom*, R1400E mutant. For each one, *main panel*, *solid* and *dashed lines* are the spectra recorded during steady-state NO synthesis and after NO synthesis had stopped due to NADPH depletion. They were recorded at 25 and 75 s after mixing for wild-type and at 40 and 120 s after mixing for the mutants, respectively. *Upper* and *lower insets*: absorbance changes at 436 (*solid lines*) and 340 nm (*dashed lines*) that follow ferrous heme-NO complex buildup and decay and NADPH oxidation, respectively, during the initial phase of the reaction and over the entire time course. Traces are an average of three to five individual scans.

TABLE SIX

Kinetics of ferrous heme-NO formation after initiating NO synthesis by wild-type nNOS and the Arg^{1400} mutants

Reactions were carried out in the stopped-flow spectrophotometer at 10 °C. Aerobic enzyme solutions were rapidly mixed with a buffer solution containing NADPH to start the reactions. Heme-NO complex buildup was followed at 436 nm and fit to a double exponential function to generate two rate constants (k_1 and k_2). The values are the mean ± S.D. of five to six runs representative of three to four independent measurements using two enzyme preparations. The numbers in parentheses indicate the percentage of absorbance change for each phase. Measurements and analysis are detailed under "Experimental Procedures."

nNOSfl enzyme	Ferrous heme-NO complex formation	
	k_1	k_2
	s^{-1}	
Wild-type	11.1 ± 1.5 (58%)	1.35 ± 0.06 (42%)
R1400S	18.4 ± 3.8 (73%)	1.38 ± 0.05 (27%)
R1400E	18.9 ± 4.5 (74%)	1.34 ± 0.06 (26%)

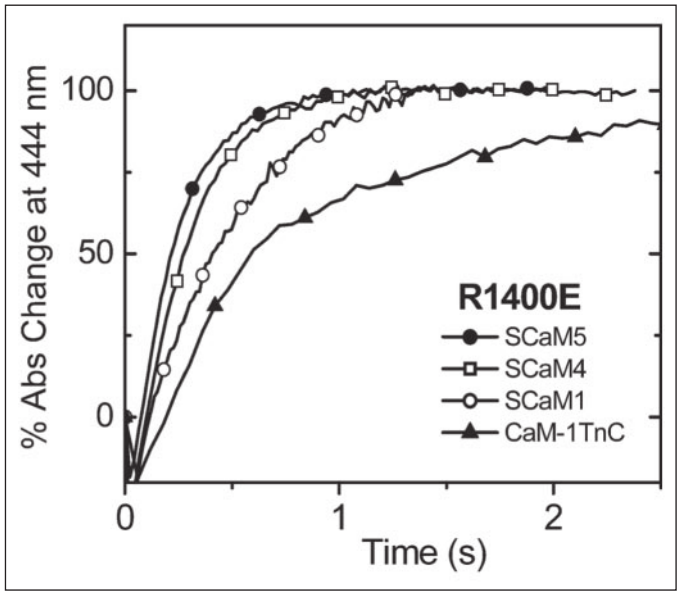

FIGURE 9. **Soybean CaM proteins and chimeras support different rates of ferric heme reduction in R1400E nNOS.** R1400E nNOS containing each indicated bound soybean CaM protein or CaM-troponin C chimera was mixed at 10 °C with excess NADPH under anaerobic, CO-saturated conditions in a stopped-flow spectrophotometer as described under "Experimental Procedures." The rate of heme iron reduction was determined by following ferrous heme-CO complex formation at 444 nm. The experimental traces shown are an average of five to eight individual scans and are representative of at least two independent experiments.

and over the entire reaction. There was a deflection in the rate of NADPH consumption concurrent with the buildup of the ferrous heme-NO complex in all three enzyme reactions, consistent with earlier results (57, 61). In all cases heme-NO complex buildup was best fit by a two-exponential function, and the rates are listed in TABLE SIX. The first phase of heme-NO complex formation was considerably faster in the mutant enzyme reactions, consistent with their increased rates of ferric heme reduction and NO biosynthesis. This was associated with faster initial rates of NADPH oxidation in the mutants (data not shown).

NO Synthesis Supported by CaM Substitutes—The above data establish that the lower NO synthesis activities of the Arg^{1400} mutants are associated with faster rates of ferric heme reduction and catalysis, as we have found for other nNOS mutants (56). Native soybean CaM proteins (SCaM) and CaM-cardiac troponin c chimeras (CaMTnC) bind to nNOS with good affinity and support different rates of ferric heme reduction in nNOS (16, 56, 62). We therefore used a human CaM M144V mutant, SCaM proteins (SCaM-1, SCaM-1 V144M point mutant, SCaM-4, and SCaM-5), and the CaM1TnC chimera to support a range of ferric heme reduction rates in the wild-type nNOS and Arg^{1400}E mutant and then determined how their steady-state NO synthesis activities varied as a function of the ferric heme reduction rate. Fig. 9 contains representative kinetic traces recorded at 444 nm that illustrate the different rates of ferric heme reduction that are supported by the different CaM proteins in R1400E nNOS. TABLE SEVEN lists all of the heme reduction rates that we measured along with the corresponding steady-state NO synthesis activities. The relationship between steady-state NO synthesis activity and ferric heme reduction rate for each of the two enzymes is shown as a graph in Fig. 10.

TABLE SEVEN

Steady-state NO synthesis activities and ferric heme reduction rates supported by different calmodulin proteins for wild-type nNOS and the R1400E mutant

The NO synthesis activities were measured at room temperature using the oxyhemoglobin assay and the rates of heme reduction were measured in the stopped-flow instrument at 10 °C. Each experiment was performed in triplicate, and the values are representative of two or more determinations with independent enzyme preparations.

Calmodulin type	NO synthesis from Arg		Heme reduction	
	wt	R1400E	wt	R1400E
	min^{-1}		s^{-1}	
Human CaM	52 ± 2	29 ± 2	3.9 ± 0.1	5.1 ± 0.3
SCaM5	46 ± 3	49 ± 4	3.4 ± 0.2	3.9 ± 0.4
SCaM4	44 ± 3	46 ± 3	3.3 ± 0.2	3.7 ± 0.3
SCaM1 V144M	32 ± 4	37 ± 3	3.0 ± 0.1	3.5 ± 0.2
HCaM M144V	20 ± 2	30 ± 3	2.1 ± 0.1	3.1 ± 0.2
SCaM1	22 ± 2	26 ± 2	2.3 ± 0.2	2.6 ± 0.3
CaM-1TnC	10 ± 3	20 ± 1	0.5 ± 0.2	1.6 ± 0.4

The various CaM proteins showed a similar trend in the wild-type and R1400E nNOS, with native CaM supporting the fastest rate of heme reduction in both enzymes. However, each CaM protein supported a faster rate of heme reduction in the R1400E mutant compared with wild-type. Regarding steady-state NO synthesis, wild-type nNOS achieved its greatest rate with CaM, whereas R1400E nNOS achieved its highest activity with up to three CaM substitutes that supported slower rates of heme reduction than native CaM. The data in Fig. 10 indicate that the R1400E mutation causes CaM to support a rate of ferric heme reduction that is beyond the optimal value for the steady-state NO synthesis activity of nNOS. However, CaM substitute proteins slow the rate of ferric heme reduction in R1400E nNOS such that it achieves optimal NO synthesis activity in the steady state.

DISCUSSION

The electron transfer reactions of nNOS are regulated by bound NADP(H) and the C-terminal tail (32, 42), but the mechanisms are unclear. The recently determined crystal structure of an intact nNOSr identified an ionic interaction between the 2′-P_i of bound NADP(H) and a C-terminal tail residue (Arg^{1400}) that potentially links their mechanisms of action (30). Our current results confirm this model and establish a role for the Arg^{1400}-2′-P_i interaction in repressing the electron transfer activities of nNOS. Perhaps the hallmark is in how the interaction impacts the cytochrome *c* reductase activity of CaM-free nNOSr. When the interaction was eliminated (by means of the R1400S mutant or by using NADH in place of NADPH), or was converted to a repelling interaction (the R1400E mutant), it led to increased cytochrome *c* reductase activities and partly relieved the catalytic repression that is

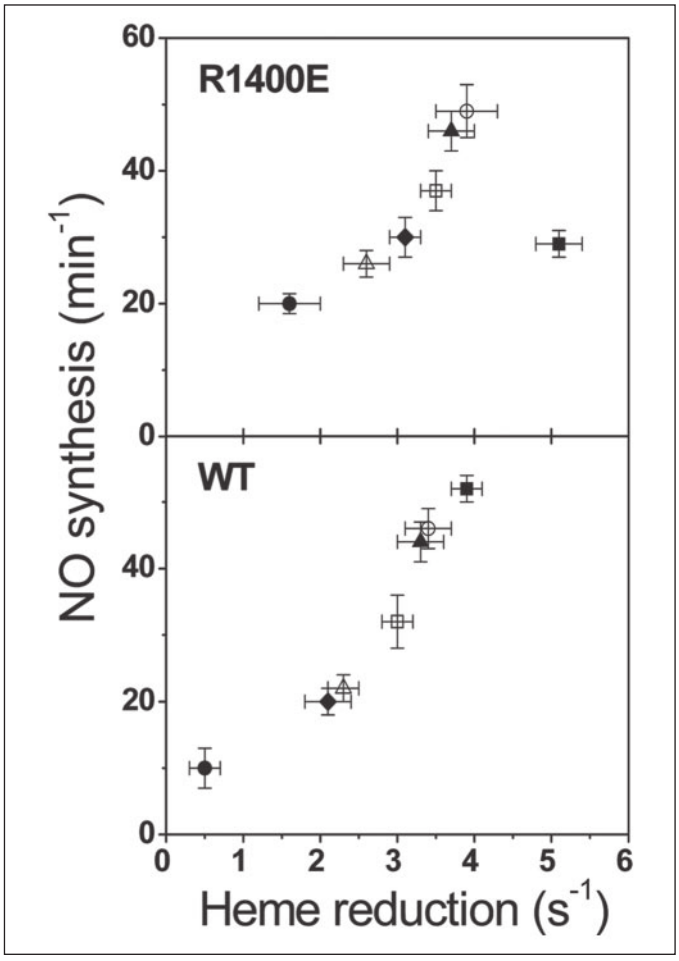

FIGURE 10. **Relationship between the steady-state NO synthesis activity and ferric heme reduction rate in R1400E and wild-type nNOS.** Points are the mean values ± S.D. for the NO synthesis activities and heme reduction rates listed in TABLE SEVEN. CaM (■), SCaM5(○), SCaM4 (▲), SCaM1 V144M (□), CaM M144V (◆), SCaM-1 (△), and CaM-1TnC (●) are shown.

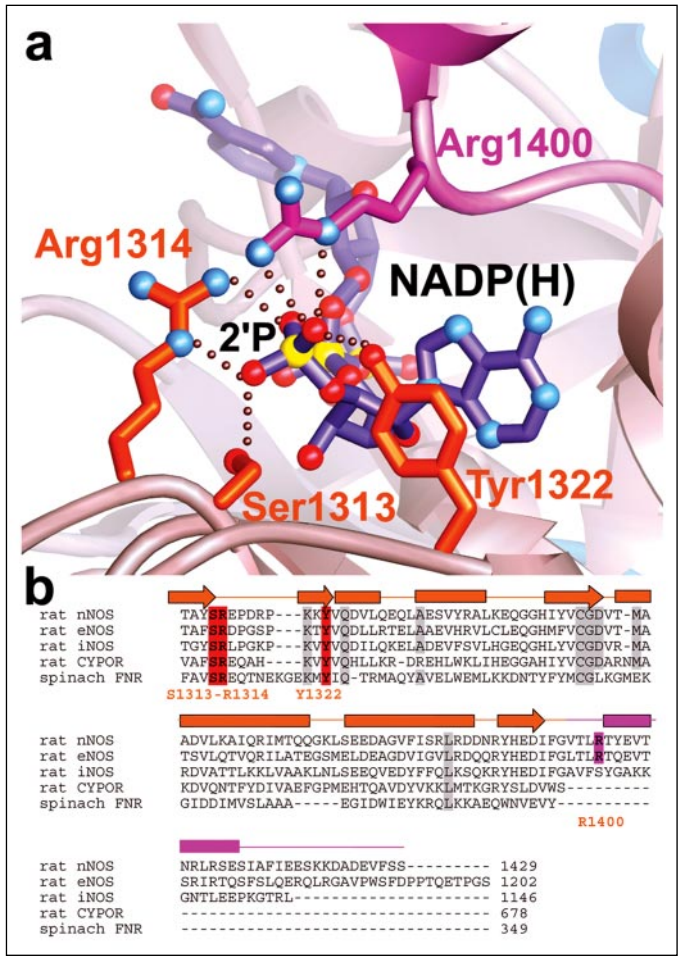

FIGURE 11. **Residues that interact with the 2′-P_i of bound NADP(H) in nNOSr.** *a*, Arg^{1400} is one of four residues that interact with the 2′-P_i of bound NADP(H). *b*, structure-based alignment of the amino acid sequences of rat nNOS, eNOS, iNOS, and related flavoproteins FNR and cytochrome P450 reductase (*CYPOR*) in the NADPH binding region showing the position of the NADPH interactions. The nNOS residues Tyr^{1322}, Arg^{1314}, and Ser^{1313} (marked in *red*) represent a triad whose identity is conserved among the FNR family of flavoproteins, whereas Arg^{1400} is unique to nNOS and eNOS.

normally present in CaM-free nNOSr.[3] To understand how the Arg^{1400}-2′-P_i interaction helps to regulate nNOS, we examined its influence on several events that underlie electron transfer and catalysis, as discussed below.

NADP(H) Interaction—On the basis of work with related flavoproteins (63–66), NADP(H) binding within the FNR module of nNOS is thought to occur in a bipartite mode, with the nicotinamide ring engaging in an aromatic stacking interaction with the FAD isoalloxazine ring, and the 2′,5′-ADP moiety making ionic and hydrogen bonding interactions with conserved residues in other areas of the FNR module (22, 30). Invariably, most of the binding energy is attributed to the 2′,5′-ADP interaction in these enzymes (25). On the basis of our K_m measurements, Arg^{1400} may have relatively little impact on NADP(H) binding in nNOS. This makes sense, given that Arg^{1400} is only one of four residues that interact with the 2′-P_i of NADP(H) (Fig. 11*A*). The three other residues (Tyr^{1322}, Arg^{1314}, and Ser^{1313} in nNOS) represent a triad whose identity and function in binding the 2′-P_i group are conserved among the FNR family of flavoproteins (Fig. 11*B*). Mutagenesis studies have confirmed the importance of the triad residues in determining NADP(H) binding affinity and selectivity *versus* NADH in related flavoproteins (64, 67). It is likely that the triad residues have similar function in nNOS, although this remains to be directly demonstrated.

Given the high mobility of the C-terminal tail (30, 42, 56) and the weak conservation of Arg^{1400} among NOSs (it is Ser in iNOS), it seems plausible that NOS enzymes would not rely on Arg^{1400} for their NADP(H) binding affinity and selectivity. But could modest changes in the NADP(H) interaction be sufficient to relieve the repression of cytochrome *c* reductase activity under CaM-free conditions in the Arg^{1400} mutants? On the basis of their increased K_m values, the Arg^{1400} mutants may have increased rates of $NADP^+$ dissociation relative to wild-type nNOS. The rate of $NADP^+$ dissociation has been suggested as a possible rate-limiting step for cytochrome *c* reduction (58). Unfortunately, our attempts to measure the K_d for $NADP^+$ using a spectral perturbation method (34) were thwarted by our observing relatively small absorbance changes upon $NADP^+$ binding to the Arg^{1400} mutants (data not shown). The rate of $NADP^+$ dissociation has only been measured for the oxidized wild-type nNOSr (34) and was found to be about 3 times faster than the steady-state rate of electron transfer to cytochrome *c* measured at the same temperature. This suggests that any increase in the rate of $NADP^+$ dissociation that might be caused by the Arg^{1400} mutations may not impact the steady-state rate of cytochrome *c* reduction, because $NADP^+$ release from nNOSr is relatively fast. On the other

[3] The increased cytochrome *c* reductase activities were not simply due to a mutational effect on apparent K_m, because the concentration of cytochrome *c* in the assays far exceeds the enzyme apparent K_m for cytochrome *c*.

hand, $NADP^+$ may dissociate more slowly from partially reduced forms of nNOSr. Clearly, questions regarding the $NADP^+$ release rate are fundamental to nNOSr catalysis and deserve further investigation. We suspect, however, that changes in NADP(H) interaction are probably not responsible for relieving the catalytic repression as seen in the CaM-free Arg^{1400} mutant enzymes.

Flavin Reduction Kinetics—We observed increased rates of flavin reduction in our CaM-free Arg^{1400} mutants relative to wild-type, implying that the Arg^{1400}-NADP(H) interaction helps to repress flavin reduction kinetics in CaM-free nNOS. Interestingly, deletion of the C-terminal tail also increased the flavin reduction rate in CaM-free nNOS (42). The mechanism and physical basis for the rate enhancement is difficult to envision, and will require further study. Could the increased flavin reduction rates underlie the greater cytochrome *c* reductase activities of our CaM-free Arg^{1400} mutants? Available data suggest that hydride transfer from NADPH to FAD is relatively fast in nNOS and does not limit electron transfer from nNOS to cytochrome *c* under any circumstance (17, 32, 34, 68, 69). In addition, although an increased flavin reduction rate in nNOS is often associated with increased cytochrome *c* reductase activities (28, 59, 70), this association is not absolute, because some nNOS mutants have increased cytochrome *c* reductase activity while maintaining a flavin reduction rate that is equivalent to that in CaM-free wild-type nNOS (34). Craig *et al.* (32) have also argued that inter-flavin electron transfer steps are not rate-limiting for cytochrome *c* reduction based on data obtained in nNOSr oxidation reactions with cytochrome *c*. However, other data suggest electron transfer between the FAD and FMN groups may limit cytochrome *c* reduction by nNOS (71). Thus, it remains possible that the faster rates of flavin reduction could contribute toward the greater cytochrome *c* reductase activities of the CaM-free Arg^{1400} mutants.

Conformational Equilibrium of nNOSr—Craig *et al.* (32) first showed that bound NADP(H) was required to repress electron transfer to cytochrome *c* by CaM-free nNOSr, and proposed that it did so by locking nNOSr in a conformation that diminished or prevented the reaction of its FMN module with external electron acceptors. The nNOSr crystal structure (30) subsequently revealed that the C-terminal tail was positioned to regulate the conformational freedom of the FMN module (Fig. 1*B*), and implicated the Arg^{1400}-NADP(H) interaction in stabilizing a "shielded" conformation for the FMN module (Fig. 1*C*). Our single turnover cytochrome *c* reduction data establish that the Arg^{1400}-2′-P_i interaction is required to stabilize the FMN module in its shielded conformation when NADP(H) binds to CaM-free nNOSr. We found that adding NADPH to wild-type nNOSr diminished the reactivity of its FMN hydroquinone with cytochrome *c*, and this repression was relieved by CaM, consistent with previous reports (32, 34). In contrast, adding NADP(H) to CaM-free R1400S nNOSr had no net effect on the reactivity of its FMN hydroquinone toward cytochrome *c*, and when NADP(H) was added to CaM-free R1400E nNOSr, it greatly increased its FMN hydroquinone reactivity. This enabling effect of the Arg^{1400}Glu mutation may arise from its allowing a charge repulsion between the side-chain carboxylate of the Glu1400 and the 2′-P_i of bound NADP(H). Such charge repulsion is expected to develop whenever the C-terminal tail interacts with the NADP(H)-bound FNR module as depicted in the nNOSr crystal structure (Fig. 1*C*). Apparently, this repulsion prevents the C-terminal tail from holding down the FMN module, and thus shifts the conformational equilibrium of the FMN module toward the deshielded state (Fig. 1*A*). The relatively weaker effect of the Arg^{1400}Ser mutation is consistent with its simply neutralizing the Arg^{1400}-NADP(H) charge-pairing interaction, rather than creating a repulsive ionic interaction.

Although it is remarkable that the FMN module becomes deshielded when NADP(H) binds to CaM-free R1400E nNOSr, this response is not unique, because it also occurs when NADP(H) binds to the F1395S nNOSr mutant (34). Phe^{1395} lies just before the start of the C-terminal tail, and its side-chain phenyl group is expected to undergo significant movement upon NADP(H) binding so that a nicotinamide-FAD stacking interaction can occur that is required for hydride transfer (22, 24, 27). Previous results suggest that the Phe^{1395} side chain is important for regulating the conformational equilibrium of the FMN module in nNOSr, because Phe^{1395} must be present to stabilize the FMN-shielded conformation and repress electron transfer when NADP(H) binds (33, 34, 65). Indeed, these data imply that Phe^{1395} is required for the Arg^{1400}-NADPH interaction to be effective. Perhaps in the absence of the phenyl side chain (*i.e.* in F1395S nNOSr) the C-terminal tail is perturbed to the point where its Arg^{1400} residue can no longer interact with an NADP(H) molecule that is bound in the FNR module. However, this simple non-interaction cannot explain why NADP(H) binding causes greater FMN deshielding in F1395S nNOSr relative to the NADPH-free enzyme (34). In any case, we now know that the conformational equilibrium of the FMN module is regulated by at least two residues of nNOSr (Phe^{1395} and Arg^{1400}) and may involve both the nicotinamide and 2′-P_i moieties of bound NADP(H). Beyond this, the nNOSr crystal structure (30) has identified a number of amino acids that create salt bridge, hydrophobic, and H-bond interactions between the FMN and FNR modules. These interactions probably help to establish a set point for the conformational equilibrium of the FMN module, and their influence on the equilibrium may or may not be sensitive to NADP(H) binding. These possibilities can now be investigated.

Can decreased shielding of the FMN module explain why the Arg^{1400} mutants have greater cytochrome *c* reductase activities than wild-type nNOSr in the CaM-free state? The evidence suggests that it can. For example, there is a strong inverse correlation between the degree of FMN shielding and the steady-state cytochrome *c* reductase activities of wild-type nNOSr, full-length nNOS (55), the R1400S and R1400E nNOSr mutants, and the F1395S nNOSr mutant (34), both in the presence or absence of CaM. In contrast, other potentially rate-limiting processes, like the rates of flavin reduction or $NADP^+$ dissociation, are either too fast relative to the enzyme activity or do not always change in correlation with the cytochrome *c* reductase activity under various conditions. Thus, our current data support a model where electron transfer to cytochrome *c* is primarily regulated by conformational gating of the FMN module of nNOS (32, 34), particularly in the CaM-free state. Although this model generally holds for the CaM-bound state as well, it is important to note that we did not observe a further increase in the cytochrome *c* reductase activity for R1400E nNOSr beyond the activity of CaM-bound wild-type nNOSr, despite evidence indicating that the FMN module in the R1400E mutant is less shielded than in CaM-bound wild-type (see Fig. 5). This discrepancy could indicate that another step in steady-state cytochrome *c* reduction becomes rate-limiting under this circumstance, such that a greater degree of FMN deshielding cannot increase the steady-state catalytic activity beyond what is already achieved by CaM binding. Further work can address this possibility.

NADP(H) Interactions That Regulate Flavoprotein Function—The ability of NADP(H) to repress electron transfer through a specific interaction of its 2′-P_i group is unusual, and may be restricted to NOS enzymes in their CaM-free state. Bound NADP(H) has additional effects on NOS and on related flavoproteins. For example, bound $NADP^+$ increases the effective midpoint potential of the FAD hydroquinone/semiquinone couple in nNOS (29) and in FNR enzymes (63). NADP(H) and 2′,5′-ADP have also been shown to decrease the affinity

of FNR enzymes toward their ferredoxin or flavodoxin electron transfer partners (72, 73). It is unclear whether this involves interactions of the 2′-P_i group with the FNR enzymes. In nNOSr, the analogous effect would have NADP(H) altering the stability of the transient complex that forms between its FNR and FMN modules (as depicted in the nNOSr crystal structure (Fig. 1*B*)). As noted here and elsewhere (30, 34), this complex likely represents the shielded conformation of the FMN module. We cannot study the strength of this interaction by traditional K_d determination, because the FNR and FMN modules of nNOSr reside on the same polypeptide. But on the basis of our FMN shielding data we can surmise how bound NADP(H) impacts the stability of the complex formed by the FNR and FMN modules. In wild-type nNOSr, the Arg^{1400}-2′-P_i interaction enables NADP(H) to stabilize the complex, exactly the opposite of what is observed for the FNR enzymes. Interestingly, in our mutant that lacks the Arg^{1400}-2′-P_i interaction (R1400S nNOSr), NADP(H) no longer stabilizes the shielded complex, but it also does not destabilize the complex, again in contrast to the FNR enzymes. This implies that nNOS has diverged from FNR enzymes in its response to NADP(H) binding. In the case of the R1400E mutant, NADP(H) does destabilize the module complex between FNR and FMN. As noted previously, this could be due to the mutation introducing a charge-repelling interaction between the 2′-P_i group and the C-terminal tail. Indeed, the C-terminal tail is a complicating factor in the analysis, and it would be valuable to perform similar studies with nNOSr mutants that lack the C-terminal tail. At this point, our data suggest that NADP(H) binding impacts nNOSr in a ways that may be unique among the FNR family of flavoproteins.

Ferric Heme Reduction and NO Synthesis in the CaM-free nNOS—Working with full-length nNOS proteins allowed us to examine how the Arg^{1400} mutations impact FMN electron transfer to the ferric heme. In the CaM-free enzymes there was no correlation between the degree of FMN shielding and the capacity to reduce the ferric heme. Both Arg^{1400} mutants had no detectable NO synthesis in the CaM-free state, and thus no ferric heme reduction, despite their containing relatively deshielded FMN modules. This was particularly remarkable for the CaM-free R1400E mutant, because its FMN module appears to be deshielded to an equal or greater extent than in CaM-bound nNOS. We can conclude that shifting the conformational equilibrium of the FMN module toward a more deshielded state is not sufficient to enable ferric heme reduction in CaM-free nNOS. Apparently, additional structural changes brought on by CaM must allow an interaction of the FMN module and the oxygenase domain that is productive for electron transfer. Indeed, ferric heme reduction in NOS may not even require the equilibrium to shift toward a less shielded FMN module, given how slow the rates of ferric heme reduction are in the NOS enzymes (61, 74, 75). The properties of the Arg^{1400} nNOS mutants are reminiscent of results obtained using Ca^{2+}-binding mutants of CaM (52, 76), plant CaM proteins (56), and CaM-TnC chimeras (31, 62), which indicate that certain domains of CaM can increase the cytochrome *c* reductase activity of NOS while supporting little or no NO synthesis. It would be interesting to determine if this behavior correlates with shifts in the conformational equilibrium of the FMN module as we observed in the present study. It is also important to note that other mutations do enable ferric heme reduction in CaM-free nNOS. For example, there is detectable heme reduction (and NO synthesis) in CaM-free F1395S nNOS (33) and in nNOS mutants that lack the C-terminal tail (42), but not in S1412D nNOS (56). The physical basis for these differences awaits further investigation.

The CaM-free Arg^{1400} nNOS mutants have higher NADPH oxidase activities than wild-type nNOS, consistent with the mutants having faster rates of flavin auto-oxidation. This phenomenon was originally reported for an nNOS whose C-terminal tail was deleted (42). Our results confirm the importance of the C-terminal tail in protecting against flavin auto-oxidation and suggest that it does so by virtue of the Arg^{1400}-NADP(H) interaction. A requirement for bound NADP(H) is an interesting possibility that should be explored. Increased flavin auto-oxidation in the Arg^{1400} mutants cannot solely be due to decreased shielding of the FMN module, because flavin auto-oxidation in nNOSr does not increase when CaM binds (34, 42), despite CaM causing a similar extent of FMN deshielding. Perhaps the Arg^{1400} mutants have greater solvent exposure of their FAD hydroquinone and semiquinone species due to a malfunctioning C-terminal tail.

Ferric Heme Reduction and NO Synthesis in the CaM-bound nNOS—Both Arg^{1400} mutants had increased rates of ferric heme reduction relative to wild-type nNOS in the CaM-bound state. The Arg^{1400} mutants also had faster rates of ferric heme reduction during catalysis, as judged by their having faster buildup of the ferrous heme-NO complex in the initial phase of their NO biosynthesis reactions (see Fig. 8). Because ferric heme reduction is rate-limiting for NO biosynthesis, a more rapid ferrous heme-NO complex formation is consistent with faster ferric heme reduction than in wild-type (37, 56). The Arg^{1400} mutants also displayed a characteristic of faster heme reduction in nNOS, namely, a diminished steady-state NO synthesis activity that can be brought back up to wild-type level when their rate of ferric heme reduction is incrementally decreased through the use of CaM substitute proteins. As previously discussed in detail (56, 75), this phenomenon is explained by a global catalytic model that has nNOS enzyme molecules partitioning between NO-releasing (productive) and NO-consuming (futile) cycles after the formation of a ferric heme-NO product complex. Because the ferric heme reduction rate in wild-type nNOS is near-optimal with regard to its enzyme partitioning, any increase in heme reduction rate through mutation (as in the Arg^{1400} mutants) creates a circumstance where a greater fraction of the ferric heme-NO product complex is reduced by the flavoprotein domain and enters the futile cycle. This causes diminished NO release detected during steady-state catalysis, despite each enzyme molecule actually synthesizing NO at a faster rate. Our current results with the Arg^{1400} mutants provide further support that nNOS is poised near its optimum rate of ferric heme reduction, and demonstrate the utility of the global model for interpreting mutant catalytic phenotypes.

We previously observed enhanced ferric heme reduction in another C-terminal tail mutant of nNOS. Specifically, the S1412D mutant, which mimics a naturally occurring phosphorylated form of nNOS in the C-terminal tail, has a rate of ferric heme reduction that is about 1.5 times that in wild-type nNOS (56). The crystal structure suggests that creating a negative charge at position Ser^{1412} should destabilize the C-terminal tail interaction with the FMN module of nNOSr (30), causing the mutant to have a less-shielded FMN module, just as we observed in the Arg^{1400} mutants. Thus, a common mechanism may explain why two separate mutations of the C-terminal tail have the same positive effect on heme reduction kinetics in CaM-bound nNOS. It will be interesting to determine if they each represent a maximal effect or if greater rate enhancements related to the C-terminal tail are still possible. But a more fundamental question is why do these mutations affect the rate of ferric heme reduction in the CaM-bound nNOS? After all, CaM binding itself prevents shielding the FMN module by the C-terminal tail and eliminates its repression of FMN electron transfer reactions. As noted previously (34), it is possible that the C-terminal tail makes unseen interactions with other structural or regulatory elements in the CaM-bound nNOS that can influence electron transfer from its FMN module to the oxygenase domain heme. But these interactions must not be essential, because NO synthesis and heme reduction still occur when CaM binds to NOS mutants that lack their C-terminal tail (41, 42, 45). In any case, enhanced heme reduction rates caused by C-terminal tail

modifications may be a natural means to regulate the NO synthesis activities of nNOS and eNOS *in vivo* (77, 78).

Acknowledgments—We thank Deborah Durra and John McDonald for excellent technical assistance, Dr. Kulwant S. Aulak for helpful advice and discussions, and Dr. Chin-Chuan Wei for assistance in CaM isoforms preparation.

REFERENCES

1. Ignarro, L. J. (2000) *Nitric Oxide: Biology and Pathobiology*, 1st Ed., Academic Press, San Diego
2. Moncada, S. (1999) *J. R. Soc. Med.* **92,** 164–169
3. Michel, T., and Feron, O. (1997) *J. Clin. Invest.* **100,** 2146–2152
4. Mize, R. R. (1998) *Nitric Oxide in Brain Development, Plasticity, and Disease*, Elsevier, New York
5. Gross, S. S., and Wolin, M. S. (1995) *Annu. Rev. Physiol.* **57,** 737–769
6. Ricciardolo, F. L., Sterk, P. J., Gaston, B., and Folkerts, G. (2004) *Physiol. Rev.* **84,** 731–765
7. Ignarro, L. J., and Napoli, C. (2005) *Curr. Diab. Rep.* **5,** 17–23
8. Stuehr, D. J. (1997) *Annu. Rev. Pharmacol. Toxicol.* **37,** 339–359
9. Masters, B. S., McMillan, K., Sheta, E. A., Nishimura, J. S., Roman, L. J., and Martasek, P. (1996) *FASEB J.* **10,** 552–558
10. Stuehr, D. J. (1999) *Biochim. Biophys. Acta* **1411,** 217–230
11. Alderton, W. K., Cooper, C. E., and Knowles, R. G. (2001) *Biochem. J.* **357,** 593–615
12. Zhang, M., and Vogel, H. J. (1994) *J. Biol. Chem.* **269,** 981–985
13. Aoyagi, M., Arvai, A. S., Tainer, J. A., and Getzoff, E. D. (2003) *EMBO J.* **22,** 766–775
14. Abu-Soud, H. M., and Stuehr, D. J. (1993) *Proc. Natl. Acad. Sci. U. S. A.* **90,** 10769–10772
15. Abu-Soud, H. M., Yoho, L. L., and Stuehr, D. J. (1994) *J. Biol. Chem.* **269,** 32047–32050
16. Panda, K., Ghosh, S., and Stuehr, D. J. (2001) *J. Biol. Chem.* **276,** 23349–23356
17. Daff, S., Noble, M. A., Craig, D. H., Rivers, S. L., Chapman, S. K., Munro, A. W., Fujiwara, S., Rozhkova, E., Sagami, I., and Shimizu, T. (2001) *Biochem. Soc Trans* **29,** 147–152
18. Sagami, I., Daff, S., and Shimizu, T. (2001) *J. Biol. Chem.* **276,** 30036–30042
19. Wei, C. C., Crane, B. R., and Stuehr, D. J. (2003) *Chem. Rev.* **103,** 2365–2383
20. Hurshman, A. R., and Marletta, M. A. (2002) *Biochemistry* **41,** 3439–3456
21. Bredt, D. S., Hwang, P. M., Glatt, C. E., Lowenstein, C., Reed, R. R., and Snyder, S. H. (1991) *Nature* **351,** 714–718
22. Zhang, J., Martasek, P., Paschke, R., Shea, T., Siler Masters, B. S., and Kim, J. J. (2001) *J. Biol. Chem.* **276,** 37506–37513
23. Porter, T. D. (1991) *Trends Biochem. Sci.* **16,** 154–158
24. Karplus, P. A., Daniels, M. J., and Herriott, J. R. (1991) *Science* **251,** 60–66
25. Murataliev, M. B., Feyereisen, R., and Walker, F. A. (2004) *Biochim. Biophys. Acta* **1698,** 1–26
26. Wang, M., Roberts, D. L., Paschke, R., Shea, T. M., Masters, B. S., and Kim, J. J. (1997) *Proc. Natl. Acad. Sci. U. S. A.* **94,** 8411–8416
27. Neeli, R., Roitel, O., Scrutton, N. S., and Munro, A. W. (2005) *J. Biol. Chem.* **280,** 17634–17644
28. Matsuda, H., and Iyanagi, T. (1999) *Biochim. Biophys. Acta* **1473,** 345–355
29. Garnaud, P. E., Koetsier, M., Ost, T. W., and Daff, S. (2004) *Biochemistry* **43,** 11035–11044
30. Garcin, E. D., Bruns, C. M., Lloyd, S. J., Hosfield, D. J., Tiso, M., Gachhui, R., Stuehr, D. J., Tainer, J. A., and Getzoff, E. D. (2004) *J. Biol. Chem.* **279,** 37918–37927
31. Newman, E., Spratt, D. E., Mosher, J., Cheyne, B., Montgomery, H. J., Wilson, D. L., Weinberg, J. B., Smith, S. M., Salerno, J. C., Ghosh, D. K., and Guillemette, J. G. (2004) *J. Biol. Chem.* **279,** 33547–33557
32. Craig, D. H., Chapman, S. K., and Daff, S. (2002) *J. Biol. Chem.* **277,** 33987–33994
33. Adak, S., Sharma, M., Meade, A. L., and Stuehr, D. J. (2002) *Proc. Natl. Acad. Sci. U. S. A.* **99,** 13516–13521
34. Konas, D. W., Zhu, K., Sharma, M., Aulak, K. S., Brudvig, G. W., and Stuehr, D. J. (2004) *J. Biol. Chem.* **279,** 35412–35425
35. Siddhanta, U., Presta, A., Fan, B., Wolan, D., Rousseau, D. L., and Stuehr, D. J. (1998) *J. Biol. Chem.* **273,** 18950–18958
36. Ortiz de Montellano, P. R., Nishida, C., Rodriguez-Crespo, I., and Gerber, N. (1998) *Drug Metab. Dispos.* **26,** 1185–1189
37. Adak, S., Aulak, K. S., and Stuehr, D. J. (2001) *J. Biol. Chem.* **276,** 23246–23252
38. Salerno, J. C., Harris, D. E., Irizarry, K., Patel, B., Morales, A. J., Smith, S. M., Martasek, P., Roman, L. J., Masters, B. S., Jones, C. L., Weissman, B. A., Lane, P., Liu, Q., and Gross, S. S. (1997) *J. Biol. Chem.* **272,** 29769–29777
39. Daff, S., Sagami, I., and Shimizu, T. (1999) *J. Biol. Chem.* **274,** 30589–30595
40. Knudsen, G. M., Nishida, C. R., Mooney, S. D., and Ortiz de Montellano, P. R. (2003) *J. Biol. Chem.* **278,** 31814–31824
41. Roman, L. J., Miller, R. T., de La Garza, M. A., Kim, J. J., and Masters, B. S. (2000) *J. Biol. Chem.* **275,** 21914–21919
42. Roman, L. J., Martasek, P., Miller, R. T., Harris, D. E., de La Garza, M. A., Shea, T. M., Kim, J. J., and Masters, B. S. (2000) *J. Biol. Chem.* **275,** 29225–29232
43. Montgomery, H. J., Romanov, V., and Guillemette, J. G. (2000) *J. Biol. Chem.* **275,** 5052–5058
44. Nishida, C. R., and Ortiz de Montellano, P. R. (2001) *J. Biol. Chem.* **276,** 20116–20124
45. Lane, P., and Gross, S. S. (2002) *J. Biol. Chem.* **277,** 19087–19094
46. Chen, P. F., and Wu, K. K. (2000) *J. Biol. Chem.* **275,** 13155–13163
47. Siddhanta, U., Wu, C., Abu-Soud, H. M., Zhang, J., Ghosh, D. K., and Stuehr, D. J. (1996) *J. Biol. Chem.* **271,** 7309–7312
48. Gachhui, R., Ghosh, D. K., Wu, C., Parkinson, J., Crane, B. R., and Stuehr, D. J. (1997) *Biochemistry* **36,** 5097–5103
49. George, S. E., Su, Z., Fan, D., and Means, A. R. (1993) *J. Biol. Chem.* **268,** 25213–25220
50. George, S. E., Su, Z., Fan, D., Wang, S., and Johnson, J. D. (1996) *Biochemistry* **35,** 8307–8313
51. Su, Z., Blazing, M. A., Fan, D., and George, S. E. (1995) *J. Biol. Chem.* **270,** 29117–29122
52. Kondo, R., Tikunova, S. B., Cho, M. J., and Johnson, J. D. (1999) *J. Biol. Chem.* **274,** 36213–36218
53. Panda, K., Adak, S., Konas, D., Sharma, M., and Stuehr, D. J. (2004) *J. Biol. Chem.* **279,** 18323–18333
54. Stuehr, D. J. (1996) *Methods Enzymol.* **268,** 324–333
55. Adak, S., Ghosh, S., Abu-Soud, H. M., and Stuehr, D. J. (1999) *J. Biol. Chem.* **274,** 22313–22320
56. Adak, S., Santolini, J., Tikunova, S., Wang, Q., Johnson, J. D., and Stuehr, D. J. (2001) *J. Biol. Chem.* **276,** 1244–1252
57. Abu-Soud, H. M., Wang, J., Rousseau, D. L., Fukuto, J. M., Ignarro, L. J., and Stuehr, D. J. (1995) *J. Biol. Chem.* **270,** 22997–23006
58. Knight, K., and Scrutton, N. S. (2002) *Biochem. J.* **367,** 19–30
59. Gachhui, R., Presta, A., Bentley, D. F., Abu-Soud, H. M., McArthur, R., Brudvig, G., Ghosh, D. K., and Stuehr, D. J. (1996) *J. Biol. Chem.* **271,** 20594–20602
60. Noble, M. A., Munro, A. W., Rivers, S. L., Robledo, L., Daff, S. N., Yellowlees, L. J., Shimizu, T., Sagami, I., Guillemette, J. G., and Chapman, S. K. (1999) *Biochemistry* **38,** 16413–16418
61. Santolini, J., Adak, S., Curran, C. M., and Stuehr, D. J. (2001) *J. Biol. Chem.* **276,** 1233–1243
62. Gachhui, R., Abu-Soud, H. M., Ghosha, D. K., Presta, A., Blazing, M. A., Mayer, B., George, S. E., and Stuehr, D. J. (1998) *J. Biol. Chem.* **273,** 5451–5454
63. Batie, C. J., and Kamin, H. (1986) *J. Biol. Chem.* **261,** 11214–11223
64. Tejero, J., Martinez-Julvez, M., Mayoral, T., Luquita, A., Sanz-Aparicio, J., Hermoso, J. A., Hurley, J. K., Tollin, G., Gomez-Moreno, C., and Medina, M. (2003) *J. Biol. Chem.* **278,** 49203–49214
65. Dunford, A. J., Marshall, K. R., Munro, A. W., and Scrutton, N. S. (2004) *Eur. J. Biochem.* **271,** 2548–2560
66. Deng, Z., Aliverti, A., Zanetti, G., Arakaki, A. K., Ottado, J., Orellano, E. G., Calcaterra, N. B., Ceccarelli, E. A., Carrillo, N., and Karplus, P. A. (1999) *Nat. Struct. Biol.* **6,** 847–853
67. Martinez-Julvez, M., Tejero, J., Peregrina, J. R., Nogues, I., Frago, S., Gomez-Moreno, C., and Medina, M. (2005) *Biophys. Chem.* **115,** 219–224
68. Gutierrez, A., Lian, L. Y., Wolf, C. R., Scrutton, N. S., and Roberts, G. C. (2001) *Biochemistry* **40,** 1964–1975
69. Gutierrez, A., Munro, A. W., Grunau, A., Wolf, C. R., Scrutton, N. S., and Roberts, G. C. (2003) *Eur. J. Biochem.* **270,** 2612–2621
70. Guan, Z. W., and Iyanagi, T. (2003) *Arch. Biochem. Biophys.* **412,** 65–76
71. Guan, Z. W., Kamatani, D., Kimura, S., and Iyanagi, T. (2003) *J. Biol. Chem.* **278,** 30859–30868
72. Nogues, I., Tejero, J., Hurley, J. K., Paladini, D., Frago, S., Tollin, G., Mayhew, S. G., Gomez-Moreno, C., Ceccarelli, E. A., Carrillo, N., and Medina, M. (2004) *Biochemistry* **43,** 6127–6137
73. Batie, C. J., and Kamin, H. (1984) *J. Biol. Chem.* **259,** 8832–8839
74. Abu-Soud, H. M., Presta, A., Mayer, B., and Stuehr, D. J. (1997) *Biochemistry* **36,** 10811–10816
75. Stuehr, D. J., Santolini, J., Wang, Z. Q., Wei, C. C., and Adak, S. (2004) *J. Biol. Chem.* **279,** 36167–36170
76. Stevens-Truss, R., Beckingham, K., and Marletta, M. A. (1997) *Biochemistry* **36,** 12337–12345
77. Dimmeler, S., Fleming, I., Fisslthaler, B., Hermann, C., Busse, R., and Zeiher, A. M. (1999) *Nature* **399,** 601–605
78. Fulton, D., Fontana, J., Sowa, G., Gratton, J. P., Lin, M., Li, K. X., Michell, B., Kemp, B. E., Rodman, D., and Sessa, W. C. (2002) *J. Biol. Chem.* **277,** 4277–4284